Synthesis of Dissipative Nonlinear Controllers for Series Resonant DC/DC Converters

Aleksandar M. Stanković, *Member, IEEE,* David J. Perreault, *Member, IEEE,* and Kenji Sato, *Member, IEEE*

Abstract—This paper describes analytical advances and practical experiences in a nonlinear controller design methodology for series resonant dc/dc converters. The control goal is to maintain the output voltage (which is the only measured variable) in the presence of large-load perturbations by varying the switching frequency. The proposed methodology utilizes large-scale, nonlinear switched, and generalized averaged models, and the resulting closed-loop system is exponentially convergent under typical operating conditions. The designer has a direct handle over the convergence rate, and the nonlinear controller requires only the usual output voltage measurements, while the load variations are estimated. The control structure allows for variations in both resistive and current loads. The dissipativity-based nonlinear controller is implemented in affordable analog circuitry and evaluated experimentally.

Index Terms— Dissipative control, large-signal modeling and control, output feedback, resonant converters.

I. INTRODUCTION

THE LITERATURE on modeling and control of resonant converters is voluminous, and only references directly related to the development presented here will be reviewed. The task of modeling of a dynamic system that is to be controlled is often closely intertwined with the control synthesis approach, and this is especially true in the case of resonant dc/dc converters. Control-oriented modeling of resonant converters was the subject of [1]–[3] (for an early review, see [4]). The use of generalized averaging for the purpose of modeling series resonant dc/dc converters has been addressed in [5]–[7]. Small-signal models for series and parallel resonant converters have been derived and verified in [8]. A linear control law using the energy stored in the resonant tank has been developed in [9]. A controller that traverses an optimal trajectory in terms of the resonant tank variables has been described in [10]. Sampled-data modeling and digital control of a series resonant converter has been addressed in [4]. Robust controller design for series resonant dc/dc converters has been addressed in [11] within a linear quadratic-loop transfer recovery (LQG/LTR) methodology. The difficulty with this type of approach is in the specifications of the weighting

matrices that often require design iterations. A controller based on fuzzy logic is reported in [12]; it is based on gain scheduling to distinguish between small- and large-load changes, and requires a fast microcontroller. The use of physical and circuit-theoretic properties such as dissipativity in control design of switched-mode power converters (buck, boost, etc.) has been suggested in [13] and [14], together with Lyapunov-based techniques utilizing "energy in the increment." The same approach was extended to state and parameter estimation and applied to switched-mode converters in [15]. This paper proceeds along a similar direction, and combines control and estimation of unknown load parameters using a time-scale decomposition. The procedure presented here employs a generalization of the dissipativity-based design procedure for series resonant dc/dc converters given in [16] and [17]. The procedure described in this paper allows for both resistive and current loads and is verified in laboratory experiments that employ simple analog hardware.

The standard single-loop controller structure for a series resonant dc/dc converter is a fixed linear proportional–integral (PI) controller whose input is the deviation in the output voltage, and whose output is the change in switching frequency (denoted as "frequency control" in [10]). A linear single-loop controller has the advantages of being simple to design and easy to implement. Its main disadvantage is a fairly low-closed-loop bandwidth (for converters with switching frequency of the order of 50 kHz and with wide-load variation, the closed-loop bandwidth is often of the order of 20–40 Hz). It was shown in [18] that this problem is not accidental, as uncertainties introduced by load variations prevent the PI structure (and other fixed linear controllers of reasonable complexity) from providing both robust stability and robust performance. Bode plots presented in the next section will quantify this difficulty. High-performance solutions reported in the literature [4], [9], [10] require additional measurements of the variables in the resonant tank to overcome the problem. This paper proposes a control structure consisting of a proportional and integral part combined with a nonlinear gain to improve performance of single-loop controllers.

The main control design approach advanced here is to "shape" the stored energy of the closed-loop system (this energy will be defined precisely shortly), while achieving output voltage regulation. The presented methodology differs from the feedback linearization and similar approaches as it avoids some intrinsically nonrobust operations, such as exact cancellations of nonlinearities. The control approach utilizes the physical laws underlying energy conversion and
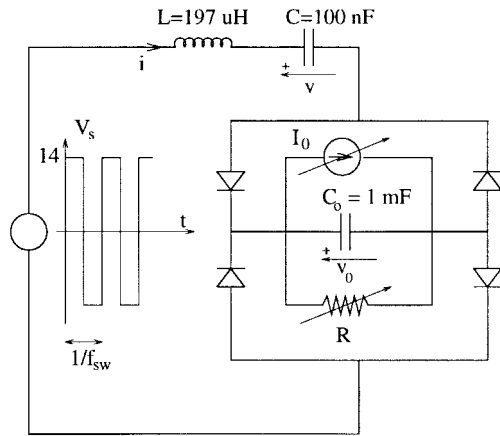
Fig. 1.   Circuit schematic of a series resonant converter.

the model structure in a fundamental way, as it consists of: 1) specification of the desired (target) energy function of the closed-loop system (which contains incremental terms around the intended operating mode, i.e., desired output voltage and estimated load), and desired (periodic) steady-state trajectories that provide output voltage regulation and 2) addition of "damping" around this nominal trajectory (i.e., dissipation of undesirable deviations of stored energy) that assures exponential convergence toward the nominal trajectory, thus guaranteeing robust operation. This control design approach is denoted as "dissipativity based" in control and robotics literature [19]; while the basic version of this control design methodology assumes measurements of all states and disturbances, an improvement that estimates the unknown, but constant (parametric) disturbance [16], [19] is applied to resonant dc/dc converters in this paper.

The paper is organized as follows. In Section II, a mathematical model of the series resonant converter is presented. In Section III, a dissipativity-based control law is designed. Simulations and laboratory tests are described in Section IV, while conclusions are outlined in Section V. A particular structural property of dynamical systems that makes them amenable to dissipativity-based design (differential flatness) is described and applied to series resonant converters in the Appendix.

II. MODELING A SERIES RESONANT CONVERTER

A series resonant dc/dc converter is shown in Fig. 1. Using the notation given in the figure, a state-space model can be written as

$$L \frac{di}{dt} = -v - v_0 \operatorname{sgn}(i) + V_s \operatorname{sgn}(\sin(\omega_s t))$$
$$C \frac{dv}{dt} = i$$
$$C_0 \frac{dv_0}{dt} = abs(i) - \frac{v_0}{R} - I_0 \qquad (1)$$

where ω_s denotes the switching frequency in rad/s, v and i are the resonant tank voltage and current, respectively, and v_0 is the output voltage supplying the load comprising a resistor R and a current sink I_0.

The model (1) can be rewritten in the form that is standard in the literature on dissipative Lagrangian (Hamiltonian) systems

[19], [20] using the state vector $x = [i \quad v \quad v_0]^T$, and the control input $u = [\omega_s \quad V_s]^T$

$$\mathcal{D}\dot{x} + \mathcal{C}(x)x + \mathcal{R}x = \mathcal{M}(u) + \mathcal{F}. \qquad (2)$$

In this representation, $\mathcal{D}$ and $\mathcal{R}$ are diagonal matrices

$$\mathcal{D} = \operatorname{diag}(L \quad C \quad C_0) \quad \mathcal{R} = \operatorname{diag}(0 \quad 0 \quad 1/R) \qquad (3)$$

and

$$\mathcal{M}(u) = [V_s \operatorname{sgn}(\sin(\omega_s t)) \quad 0 \quad 0]^\top$$
$$\mathcal{F} = [0 \quad 0 \quad -I_0]^\top$$

while $\mathcal{C}(x)$ is skew symmetric

$$\mathcal{C} = \begin{bmatrix} 0 & 1 & \operatorname{sgn}(i) \\ -1 & 0 & 0 \\ -\operatorname{sgn}(i) & 0 & 0 \end{bmatrix}$$

as it corresponds to the terms that do not affect energy storage, as $x^T \mathcal{C} x = 0$ (often denoted as "workless" terms in control literature).

An application of the dissipativity-based control is not straightforward, however, as the choice of nominal, periodic state waveforms that achieve the desired behavior of the output voltage is not apparent. To continue development of a control-oriented model, at the next step the generalized averaging procedure introduced in [5] is applied to model (1). In particular, it is assumed that both v and i are described with sufficient accuracy when their first (time-varying) harmonics are retained (denoted with V_1 and $I_1 = |I_1|e^{j\psi}$, respectively), while v_0 is assumed to be a dc quantity. It has been observed both experimentally and in numerical simulations that these assumptions are reasonable in well-designed dc/dc series resonant converters [5], [18]. (In this derivation, it is assumed that the converter switching frequency is maintained above the tank resonant frequency, so the tank current is continuous, as the resonant waveforms do not have the time to complete a cycle before the next switching period begins [21].)

The key relationship that will enable a derivation of a (nonlinear) model for the dynamics of harmonics (illustrated here for the case of the tank capacitor voltage) is [5]

$$\frac{d}{dt}V_1(t) = \left\langle \frac{dv}{dt} \right\rangle_1 (t) - j\omega_s V_1(t) \qquad (4)$$

where V_1 denotes the time-varying Fourier coefficient evaluated from

$$V_1(t) = \langle v \rangle_1(t) = \frac{1}{T_s} \int_{t-T_s}^{t} v(\tau)e^{-j\omega_s \tau}\, d\tau \qquad (5)$$

and $\omega_s = 2\pi/T_s$ corresponds to the fundamental frequency of excitation.

A (nonlinear) model for the dynamics of time-varying harmonics [evaluated "locally" in time, i.e., at time t using (5)], and assuming that the switching frequency varies slowly from one switching cycle to the next, is then obtained as [5]

$$\frac{dI_1}{dt} = -j\omega_s I_1 + \frac{1}{L}\left(-V_1 - \frac{2}{\pi}V_0 e^{j\psi} - j\frac{2V_s}{\pi}\right)$$
$$\frac{dV_1}{dt} = -j\omega_s V_1 + \frac{1}{C}I_1$$
$$\frac{dV_0}{dt} = \frac{4}{C_0 \pi} abs(I_1) - \frac{V_0}{RC_0} - \frac{I_0}{C_0}. \qquad (6)$$

This model can be written in the form of a fifth-order model involving real-valued quantities, for example, by taking real and imaginary parts of the first two equations. Let $I_1 = x_1 + jx_2$, $V_1 = x_3 + jx_4$, and $V_0 = x_5$. The control input is the switching frequency $\omega_s = u_1$ (and possibly the supply voltage $V_s = u_2$); the outputs of interest are the magnitude of the dc output y_1 (and possibly magnitudes of the series tank current, denoted by y_2, and voltage, denoted by y_3). Then the model (6) becomes

$$
\begin{aligned}
\frac{dx_1}{dt} &= x_2 u_1 - \frac{x_3}{L} - \frac{2x_5}{\pi L}\frac{x_1}{\sqrt{x_1^2 + x_2^2}} \\
\frac{dx_2}{dt} &= -x_1 u_1 - \frac{x_4}{L} - \frac{2x_5}{\pi L}\frac{x_2}{\sqrt{x_1^2 + x_2^2}} - \frac{2u_2}{\pi L} \\
\frac{dx_3}{dt} &= x_4 u_1 + \frac{x_1}{C} \\
\frac{dx_4}{dt} &= -x_3 u_1 + \frac{x_2}{C} \\
\frac{dx_5}{dt} &= \frac{4}{\pi C_0}\sqrt{x_1^2 + x_2^2} - \frac{x_5}{C_0 R} - \frac{I_0}{C_0} \\
y_1 &= x_5 \\
y_2 &= \sqrt{x_1^2 + x_2^2} \\
y_3 &= \sqrt{x_3^2 + x_4^2}.
\end{aligned} \tag{7}
$$

For control design purposes, the linearization of this model (denoted with $\tilde{x}$, $\tilde{u}$, and $\tilde{y}$) will be considered around an equilibrium operating point (denoted with X, U, and Y) corresponding to fixed switching frequency and supply voltage. In the calculation of equilibrium quantities, the phasor diagram given in Fig. 2 is useful. Analysis of (6) in a steady state yields

$$
V_0 = \frac{4R}{\pi}|I_1|. \tag{8}
$$

Application of the Pythagoras theorem in the phasor diagram in Fig. 2 results in

$$
|V_1|^2\left[(1 - LC\omega_s^2)^2 + \left(\frac{8R}{\pi^2}\omega_s C\right)^2\right] = \left(\frac{2V_s}{\pi}\right)^2 \tag{9}
$$

or in terms of the steady-state tank current (assuming that the switching frequency is above the tank resonant frequency)

$$
|I_1|(LC\omega_s^2 - 1) = \frac{2\omega_s C}{\pi}\sqrt{V_s^2 - V_0^2}. \tag{10}
$$

A key simplification for implementation of the proposed control policy will involve the additional assumption that over time horizons of interest in closed-loop control $V_0(t) \approx V_{0,d}$, where $V_{0,d}$ is the desired value of the output voltage. This assumption is satisfied to a large degree because of the size of the output capacitor C_o and because of the bandwidth of the controller. Now the small-signal model corresponding to (7) can be derived around any equilibrium point by standard linearization procedures.

In Figs. 3 and 4, the Bode magnitude and phase plots, respectively, are presented from the deviations in switching frequency (expressed in per unit of the resonant frequency) to the deviations in the output dc voltage (these plots are very similar to those reported in [8]). These plots are obtained by linearizing (7) around equilibria corresponding to various
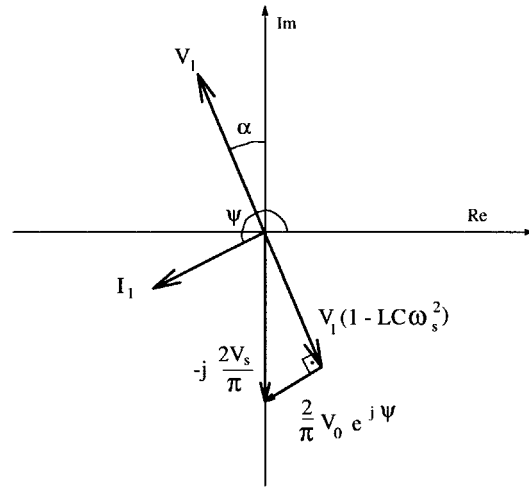

Fig. 2. Current and voltage phasor diagram at an equilibrium.

loads, and by considering the map from $\tilde{u}_1$ to $\tilde{y}_1$. The loads of interest are maximal ($R = 1$ Ω), nominal ($R = 1.6$ Ω), a typical low load ($R = 6$ Ω), and the minimal ($R = 50$ Ω, "no-load" condition). Large variations in the linearized model due to loading changes should be noted, motivating the use of robust controller design techniques. These variations prevent simple fixed linear compensators from achieving good performance over the whole operating range. Observe that the resonant peaks in the magnitude plots correspond to the difference of the resonant frequency ω_0 and the switching frequency ω_s, emphasizing the need for considering performance robustness.

III. DESIGN OF A CONTROL LAW

The qualitative analysis of dynamics of a series resonant dc/dc converter adopted here is based on the fact that variations in the tank variables are usually much faster than changes in the output voltage. This time-separation property can be established for the linearized system by using the participation factors [22], [23]. Qualitatively, the participation of the kth variable in the ℓth mode of a linear system as the amount of that mode that appears in the response of the kth variable due to an initial condition perturbation in that variable. The calculation of participation factors involves left and right eigenvectors of the system matrix, as participation factors are entries of the matrix obtained by *entry-wise* multiplication of the matrix of left eigenvectors (arranged in rows) and the matrix of right eigenvectors (arranged in columns). In the so-calculated matrix of participation factors, columns correspond to various modes and rows correspond to different states. A key property of these factors is their invariance under similarity transformations of the state vector (e.g., due to a different choice of units). At $R = 1.6$ Ω and $f_{sw} = 38$ kHz, the eigenvalues are $\lambda_{1,2} = -1630 \pm j13\,433$, $\lambda_{3,4} = -1646 \pm j464\,050$, and $\lambda_5 = -657$. The variables $\tilde{x}_1$–$\tilde{x}_4$ participate approximately equally in the complex poles (i.e., very close to 0.25 in all cases), while the output voltage $\tilde{x}_5$ participation equals 0.989 in the slowest mode λ_5. A
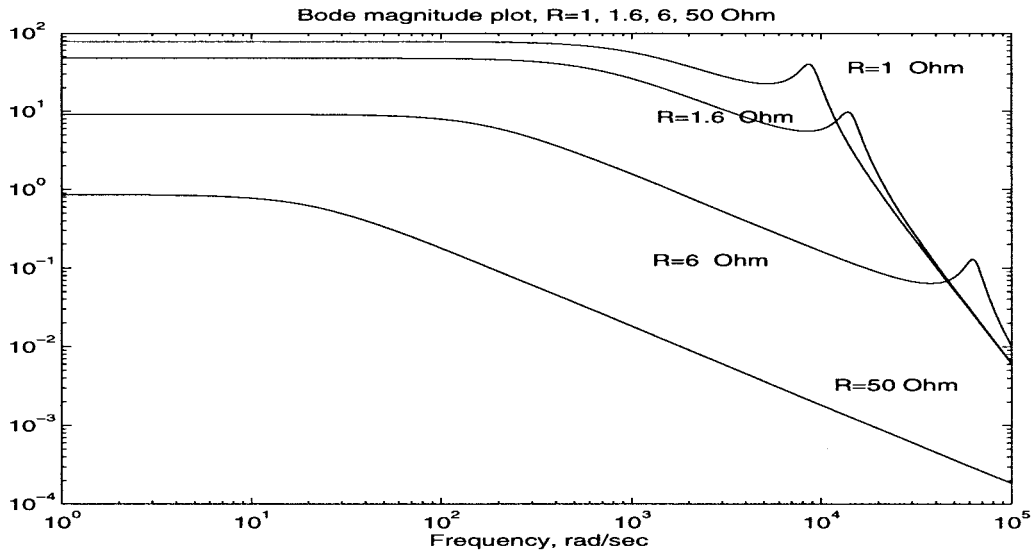
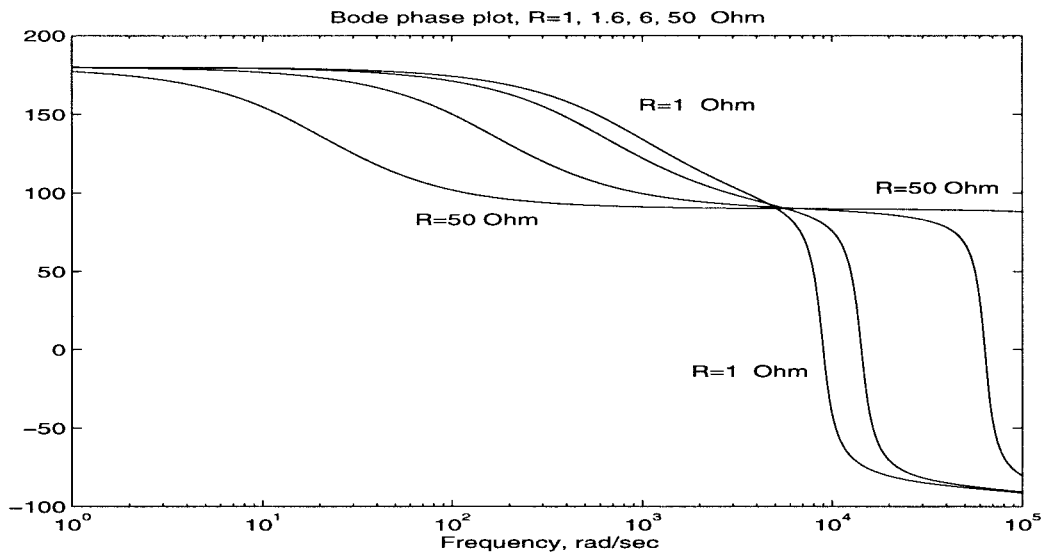Fig. 3. Bode magnitude plots for various loads.

Fig. 4. Bode phase plots for various loads.

similar statement can be made for the nonlinear model (1) using a singular perturbation argument [25], as C_0 is often substantially larger than L or C, as in the example below. This is consistent with the observation that the energy stored in the output capacitor is often an order of magnitude larger than the sum of average energies stored in the tank elements.

Motivated by this reasoning, the approach presented here follows [16] in assuming that the transients in the tank variables are instantaneous relative to the output voltage. The first step of control design is then to shape the energy stored in the output capacitor assuming the magnitude of the first harmonic of the tank current as a pseudocontrol input. Given the required value of the tank current, on the second step the corresponding switching frequency is evaluated using the steady-state relationship between the switching frequency and the magnitude of the tank current.

The main uncertainty in the operation of a series resonant dc/dc converter is the dc load that is modeled as a resistance

R in parallel with a current sink I_0 in (1). The control design problem under consideration is to synthesize a controller that will keep the dc output voltage V_0 fixed in the presence of load disturbances, i.e., changes in R and I_0.

Let $G = 1/R$ denote the conductance of the resistive load, and let $\hat{B}$ denote an estimate of a quantity B. Then, for a given reference (desired) value of the output voltage $V_{0,d}$, the error signal is defined as $e = (v_0 - V_{0,d})$, and the following quadratic function which contains error terms in the state and in load parameters is considered:

$$H_d = (1/2)C_0e^2 + \frac{V_{0,d}}{2g}(\hat{G} - G)^2 + \frac{1}{2h}(\hat{I}_0 - I_0)^2 \quad (11)$$

where g and h are positive (design) constants that are used to generate the load estimates from the available output voltage measurement

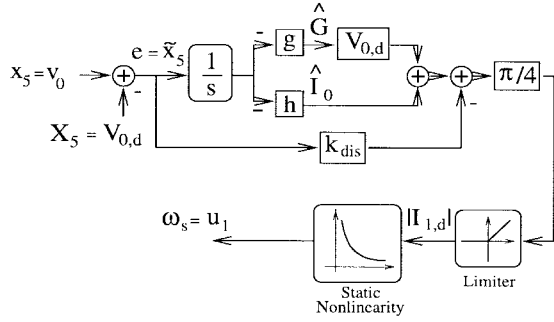$$\frac{d\hat{G}}{dt} = -ge \quad (12)$$

Fig. 5. Block diagram of the dissipative controller for a series resonant converter.

and

$$\frac{d\hat{I}_0}{dt} = -he. \tag{13}$$

Given that the first term is dimensionally (incremental) energy, the whole function is often referred to as an energy function; it may serve as a Lyapunov function if its derivative can be shown to be uniformly negative (with standard nondegeneracy conditions [24]). Recall that in this calculation we assume that the tank transient are instantaneous, so our model for e includes only the third equation of (6), with the current magnitude $abs(I_1) = |I_{1,d}|$ as the (pseudo) control input. The control design task is thus to find the $|I_{1,d}|$ to guarantee that the time derivative of H_d will be negative. Assuming that the loads G and I_0 are constant (and unknown), after calculating the derivative of (11), and taking into account the third equation in (6), (12), and (13)

$$\dot{H}_d = \frac{4}{\pi} e|I_{1,d}| - (V_{0,d}\hat{G} + \hat{I}_0)e - Ge^2. \tag{14}$$

To make the right-hand side of (14) negative, $|I_{1,d}|$ is selected to cancel the sign-indefinite terms and to add a negative term; since $|I_{1,d}|$ is nonnegative by definition, it has to be limited from below by zero

$$|I_{1,d}| = \max\left(\frac{\pi}{4}\left(V_{0,d}\hat{G} + \hat{I}_0 - k_{dis}\right)e, \, 0\right) \tag{15}$$

which results in

$$\dot{H}_d = -(G + k_{dis})e^2 \tag{16}$$

where k_{dis} is another positive design constant whose purpose is to improve the rate of convergence of H_d to zero and to make that rate less dependent on the load G. Given the pseudocontrol $|I_{1,d}|$, the actual control (switching frequency) is evaluated using the relationship which follows from (10) with $V_0 \approx V_{0,d}$

$$|I_1|(LC\omega_s^2 - 1) = \frac{2\omega_s C}{\pi}\sqrt{V_s^2 - V_{0,d}^2}. \tag{17}$$

A schematic of the proposed controller is shown in Fig. 5.

Note that this control policy establishes exponential convergence of the output voltage to its desired value. Due to issues of observability, it is not possible to guarantee that the estimates of load parameters ($\hat{G}$ and $\hat{I}_0$) used in deriving the required control input will converge to their true values. This convergence does, however, take place when only one of the
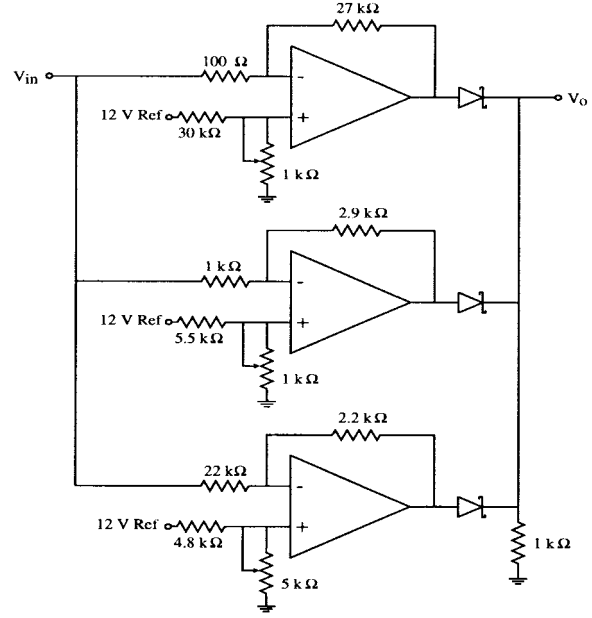

Fig. 6. Circuit implementation of the dissipative controller for a series resonant converter.

parameters is estimated (and the other one is known). If the supply voltage V_s varies parametrically (e.g., in steps with frequency that is lower than the closed-loop bandwidth), then the controller succeeds in maintaining the output voltage at $V_{0,d}$. Under those conditions parameter estimates $\hat{G}$, $\hat{I}_0$ may, however, become unreliable.

The block diagram in Fig. 5 shows that the proposed controller has a structure of a PI controller, with an added static (memoryless) nonlinearity that maps $|I_{1,d}|$ to ω_s. This suggests the possibility of an inexpensive implementation, as it will be demonstrated in the next section. Gains g, h, and k_{dis} determine characteristics of transients following load variations. A useful insight is obtained from the analysis of the linearized closed-loop system with neglected tank transients. Both the converter and the controller are first-order systems, and the adjustable gains affecting transients are shown in Fig. 5. The characteristic polynomial for a resistive load ($h = 0$) is $C_0 s^2 + (G + k_{dis})s + V_{0,d}g$. The system has two real poles (for typical component values), and the dominant pole (i.e., the one closer to the origin) approximately equals $-(V_{0,d}g)/(k_{dis} + G)$. (The approximation is based on the Taylor series expansion for the square root function and uses the fact that C_0 is much smaller than other terms in the characteristic equation.) This dominant pole should not be placed too far in the left-half plane, as tank transients may become important (recall that the corresponding fast poles $\lambda_1 - \lambda_4$, i.e., those corresponding to the tank variables, of the full model are at ≈ -1600). Note also that an increase in the proportional gain k_{dis} will lead to smaller deviations in transients, but will at the same time mandate higher values of the integral gain g (for the same speed of response). Increase in g and k_{dis} is limited by the quality of available measurements of the output voltage; in the experiments $k_{dis} = 4/\pi$ and g varies between 150–300 (so that the real part of the dominant pole is approximately between -500 and -250).
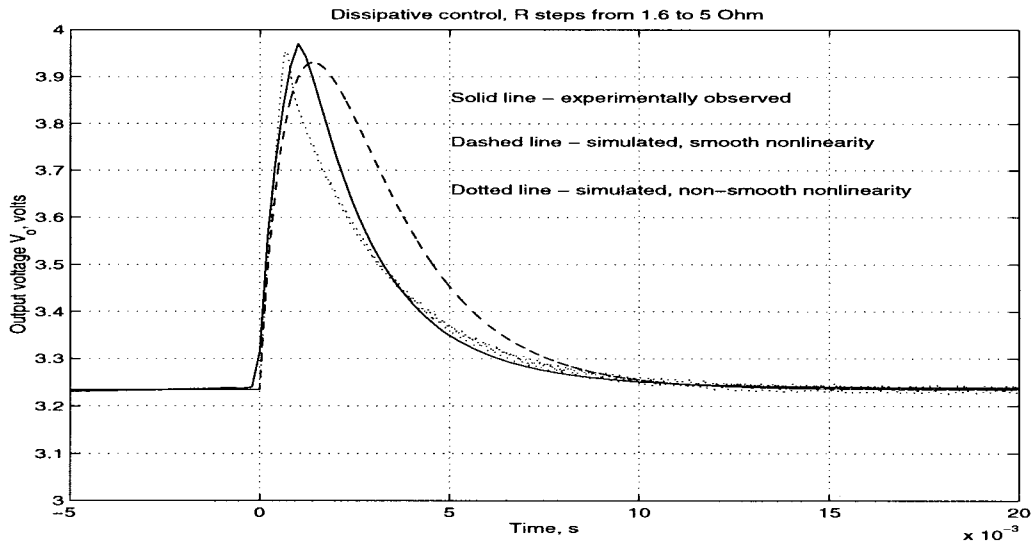
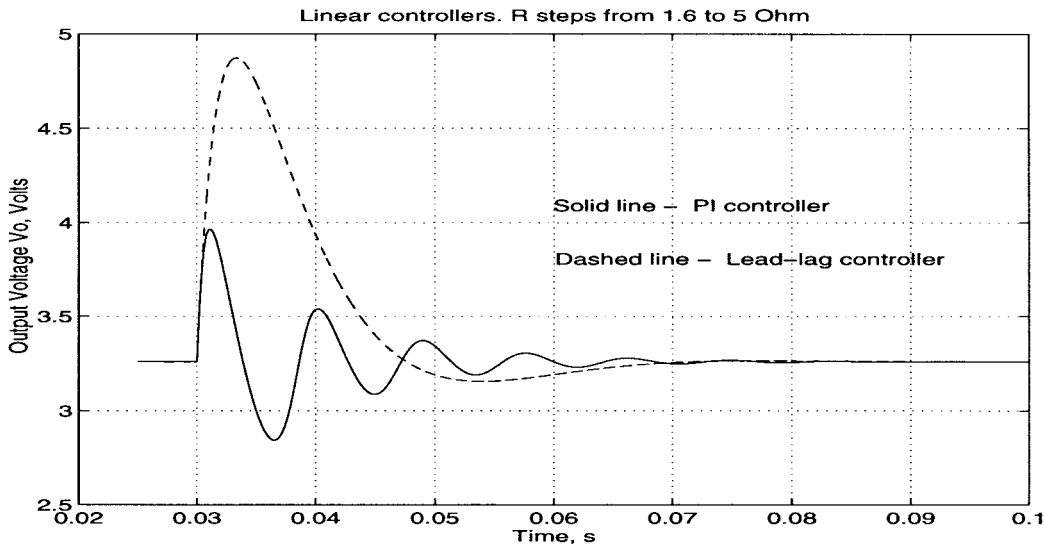Fig. 7. Comparison between experimentally observed and simulated transients in v_0 for a resistive load.

Fig. 8. Simulated responses with linear controllers: PI (solid line) and lead controller (dashed line).

IV. SIMULATIONS AND LABORATORY TESTS

A. Test Setup

The example from [5] is used to illustrate the proposed design approach, with parameter values $L = 197$ μH, $C = 100$ nF (yielding the resonant frequency of $\omega_0 = 2\pi \cdot 35$, 860), $C_0 = 1$ mF, and $V_s = 14$ V. In the case of purely resistive load, the nominal load resistance is $R = 1.6$ Ω and $\omega_s = 2\pi \cdot 38$, 110 rad/s (corresponding to $v_0 = 3.26$ V, $|V_1| = 70.25$ V, $|I_1| = 1.68$ A, and $\psi = 194.1°$). In the case of a mixed load, $I_0 = 1$ A and $R = 10$ Ω. It is assumed that the system initially operates at the nominal equilibrium, and then effects of changes in load from the nominal value are explored: 1) large-load deviation [R steps to 5 Ω, an $\approx$70% reduction in terms of power (assuming a fixed output voltage), or I_0 steps to 0.3 A, a 70% reduction]; 2) very large-load deviation in which R steps to 50 Ω (97% load power reduction, an almost complete load rejection); and 3) resistive load represented by

a pulse train, varying between 2–5 Ω, with the duty ratio 50% and frequency 50 Hz. For simulation purposes, the nonlinear model (6) has been implemented in the Simulink environment.

The controller requires load estimates $\hat{G}$ and $\hat{I}_0$ that can be readily produced with a single integrator, and the pseudocontrol $|I_1|$ can be calculated using simple circuit elements. The main challenge in a circuit implementation is in producing the switching frequency ω_s from the known (second-order) steady-state relationship (17).

The experimental power circuit uses a MOSFET-based full-bridge inverter and a Schottky diode-based rectifier. Small-series/parallel-connected film capacitors are used for the resonant capacitance, and the resonant inductor is wound on a powdered iron core. The output filter is composed of two 30-μF film capacitors in parallel with two 470-μF electrolytic capacitors. A Hewlett-Packard 6632A dc power supply is used as an input source, and a Hewlett-Packard 6060B electronic load placed in parallel with power resistors is used as a
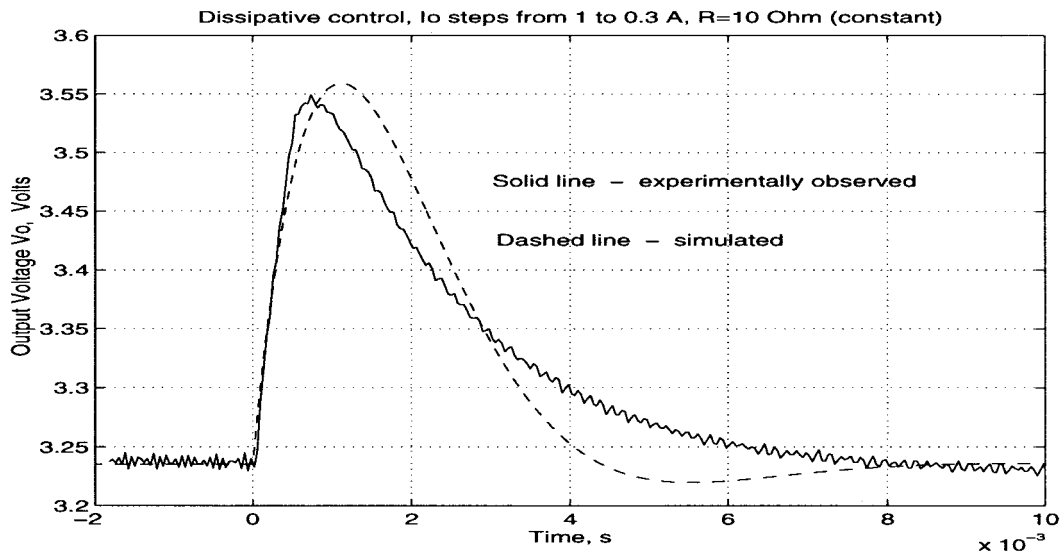
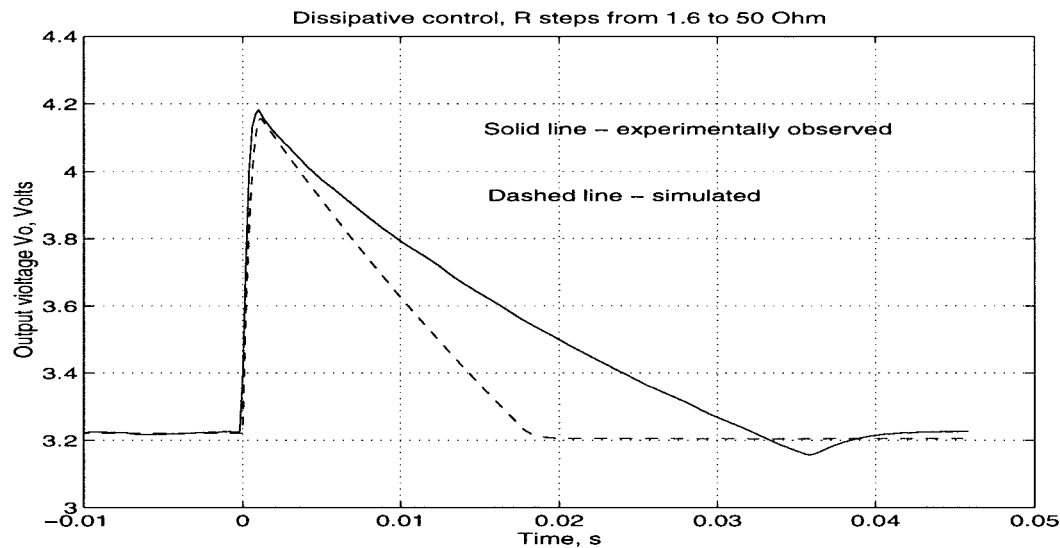Fig. 9. Comparison between experimentally observed and simulated transient in v_0 for a current load.

Fig. 10. Comparison between experimentally observed and simulated transient in v_0 for a very large change in resistive load.

load. The experimental control circuit is constructed using simple analog circuitry and closely mirrors the block diagram structure of Fig. 5. A differential amplifier is used to sense the output voltage, followed by an error amplifier which generates an error signal based on the difference between the reference voltage and the output voltage. A third opamp is connected to act as an integrator stage, while a fourth opamp (with a diode-clamped output) is connected to generate the pseudocontrol $|I_{1,d}|$ from (17). The pseudocontrol current is fed to the static nonlinearity circuit (described below), which generates a signal (V_w), which is proportional to the desired switching frequency. This signal is in turn fed to a voltage-controlled oscillator, whose output controls the power circuit gate drives.

The circuit that implements the static nonlinearity is illustrated in Fig. 6 Three opamp circuits with fixed gain and adjustable offset are joined via diodes in a logical OR connection to form the three-line approximation to the desired static nonlinearity. This implementation was selected for

experimental convenience; static nonlinearities of comparable precision can be constructed using a single amplifier and passive components. As constructed, the control circuit requires only two quad opamp packages and a voltage-controlled oscillator and could be further simplified for commercial implementation. The required level of complexity is thus on par with that of other controllers for resonant converters and does not appear to be a drawback of the approach.

B. Results

In Fig. 7, the *experimental* results for the output voltage (solid line, downloaded from a digitizing oscilloscope) are compared with simulation results [that are based on (17) and on three-line approximation], with $g = 150$ and $k_{dis} = 4/\pi$. The transient is initialized by the load change from $R = 1.6 \ \Omega$ to $R = 5 \ \Omega$. A good overall agreement can be observed, with the differences being attributable to approximations used in circuit implementation; the closed-loop bandwidth is in the order of 300 Hz.
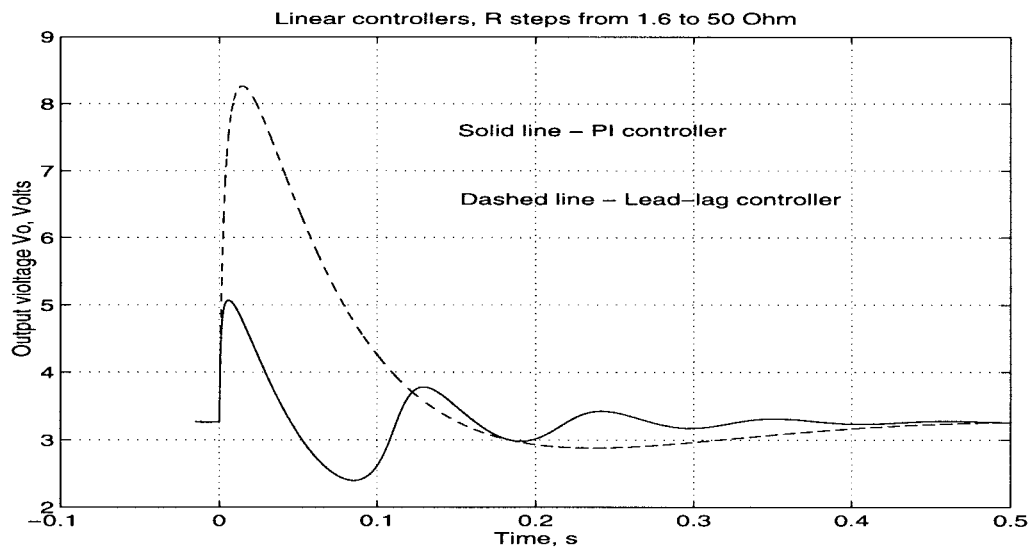
Fig. 11.   Simulated responses of a very large transient with linear controllers: PI (solid line) and lead controller (dashed line).
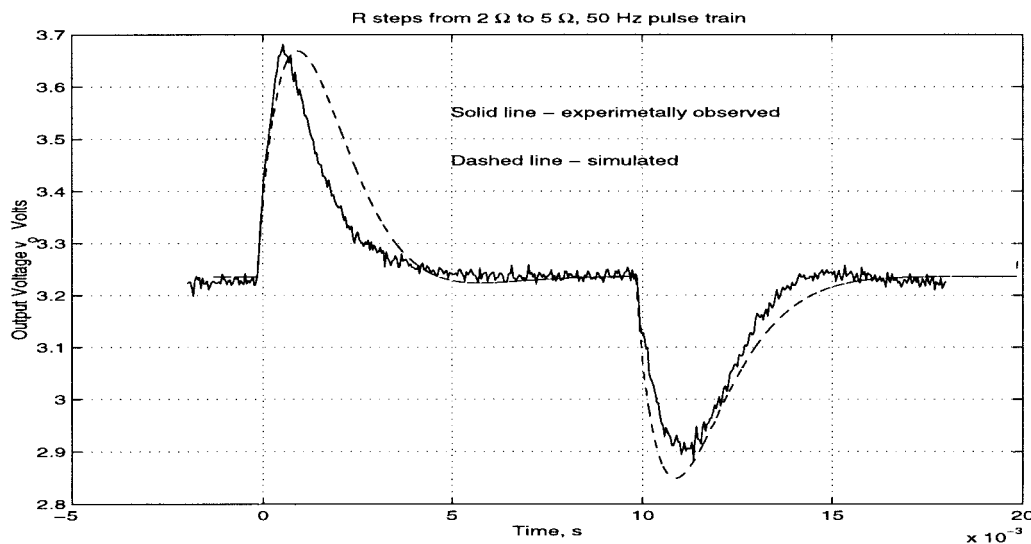

Fig. 12.   Comparison between experimentally observed and simulated transient in v_0 for a resistive 50-Hz pulse train load ($g = 300$, $k_{dis} = 1$).

Next, the performance of the dissipativity-based controller is compared with simulations with two fixed linear controllers from [18] that are presented in Fig. 8; simulations in this and in remaining plots are based on (17). One of the controllers is a PI controller with transfer function $190/(s+0.01)$, while the other is a lead-type controller obtained through a quantitative feedback theory (QFT) design methodology $3232(s + 818.4)/(s+0.01)(s+233.3 \times 10^3)$. To make the comparison fair, both designs aim to obtain a fast closed-loop response over the whole assumed range of loads. Note that the speed with which deviations in the output voltage can be eliminated is inherently limited by the output resistance forming a parallel RC_o combination, and this is especially pronounced for large R. The PI controller results in a more oscillatory response, but with smaller excursions of the output voltage [18] (in both cases the closed-loop bandwidth is of the order of 50 Hz).

Turning the attention to the case of a mixed load, in Fig. 9 the experimental results for the output voltage (solid line,

downloaded from a digitizing oscilloscope) are compared with simulation results [that are based on (17), with $h = 500$ and $k_{dis} = 1$]. The transient is initialized by the load change from $I_0 = 1$ A to $I_0 = 0.3$ A, with a constant resistive part $R = 10$ Ω. A good overall agreement is noted, with the differences again being attributable to approximations in the circuit implementation. The closed-loop bandwidth is of the order of 400 Hz.

Next, very large-load changes in which load steps from 1.6 to 50 Ω (97% load rejection) are considered. In Fig. 10, the experimental results for the output voltage (solid line) are compared with simulation results [that are based on (17), with $g = 150$ and $k_{dis} = 1$, and not on the three-line approximation]. The overall agreement, especially in terms of voltage excursion, is quite good; the approximations used in the circuit implementation are observed in the second part of the transient. The closed-loop bandwidth is in the order of 100 Hz. Next, the performance of the dissipativity-based

controller is compared with simulations using the two fixed linear controllers that are presented in Fig. 11. Observe that the closed-loop bandwidth of the linear controllers is below 10 Hz.

Finally, the case of a persistently changing load is considered, for which classical design procedures based on fixed linear controllers can provide very little guidance. The case of a resistive load pulse train [$R = R(t)$ in (7)] that changes from 2 to 5 Ω with the frequency of 50 Hz will be considered. The presented design procedure needs no modifications in this case, and experimental and simulation results are presented in Fig. 12. The difference between the two traces is again small, and attributable to the approximations involved in the circuit implementation. For comparison, the PI controller gives substantially inferior results in this case—output voltage transients are very oscillatory and span a 50% larger voltage band.

V. CONCLUSION

The control design approach presented in this paper utilizes physical insights (such as energy dissipativity) in both modeling and control synthesis, as well as time-scale separation in deriving a controller. The resulting closed-loop system is inherently robust with respect to physical uncertainties, as was demonstrated in presented experiments. The proposed dissipativity-based nonlinear controller yields a performance that is significantly improved when compared to the class of linear fixed compensators: 1) the duration of a transient is decreased close to an order of magnitude and 2) the size of the output voltage excursion is less than half of the one achievable with linear compensators of comparable complexity. The closed-loop bandwidth of dissipativity-based controllers is limited by the domain of validity of the assumed model (in which resonant tank variables are assumed to be much faster than the output voltage) and by the quality of measurements of the output voltage.

APPENDIX

The controller presented in this paper is an example of the "two degrees of freedom" control design approach: the synthesis problem is separated into: 1) design of a feasible trajectory for the nominal model and 2) regulation around that trajectory using controllers that have guaranteed performance in the presence of uncertainties and disturbances. This approach is particularly well suited for differentially flat systems: in practical terms, a system is differentially flat if a set of outputs can be found (equal in number to the number of inputs) so that all states and inputs can be determined using only algebraic relationships and differentiation [26] (note that the choice of outputs is unrestricted). While the numerical differentiation is to be avoided in practice due to noise amplification (and often is preceded with a projection to a sufficiently rich set of well-behaved functions), the property of flatness often translates into availability of computationally attractive algorithms. In other words, the property of flatness enables a replacement of analysis of (nonlinear) differential equations with analysis of (nonlinear) algebraic equations.
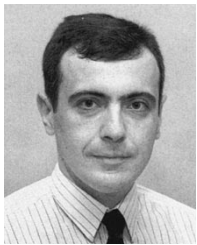
In the case of linear systems, the differential flatness is equivalent to controllability. There are, however, no systematic procedures for determining flatness of nonlinear dynamical models at this time. The differential flatness of second-order models of switched mode converters (boost and buck–boost), and their cascades has been addressed in [27].

If the (linear) model of a series resonant converter in which resonant tank dynamics are assumed to be instantaneous ("singularly perturbed" case [16]) is considered, then it turns out to be differentially flat. The "flat" output is the output voltage—with known parameters, from this output and its derivative, it is easy to recover the input. The more detailed averaged model (7) of the system is also flat if both frequency ω_s and V_s are assumed to be available control inputs (communicated to us by R. Ortega and E. Delaleau of Supelec-LSS, France).

REFERENCES

[1] V. Vorperian and S. Cuk, "Small signal analysis of resonant converters," in *Proc. IEEE PESC,* 1983, pp. 269–282.
[2] V. Vorperian, "High-Q approximation in the small signal analysis of resonant converters," in *Proc. IEEE PESC,* 1985, pp. 707–715.
[3] A. F. Witulski and R. W. Erickson, "Small signal equivalent circuit modeling of a series resonant converter," in *Proc. IEEE PESC,* 1987, pp. 693–704.
[4] M. E. Elbuluk, G. C. Verghese, and J. G. Kassakian, "Sampled-data modeling and digital control of resonant converters," *IEEE Trans. Power Electron.,* vol. 3, pp. 344–354, July 1988.
[5] S. R. Sanders, J. M. Noworolski, X. Z. Liu, and G. C. Verghese, "Generalized averaging method for power conversion circuits," *IEEE Trans. Power Electron.,* vol. 6, pp. 251–259, Apr. 1991.
[6] E. X. Yang, F. C. Lee, and M. M. Jovanovic, "Small-signal modeling of power electronic circuits using extended describing function technique," in *Proc. Virginia Power Electronics Seminar,* Sept. 1991, vol. 4, pp. 155–166.
[7] C. T. Rim and G. H. Cho, "Phasor transformation and its application to the dc/ac analysis of frequency phase-controlled series resonant converters," *IEEE Trans. Power Electron.,* vol. 5, pp. 201–211, Apr. 1990.
[8] V. Vorperian, "Approximate small-signal analysis of the series and parallel resonant converters," *IEEE Trans. Power Electron.,* vol. 4, pp. 15–24, Jan. 1989.
[9] M. G. Kim and M. J. Youn, "An energy feedback control of series resonant converters," *IEEE Trans. Power Electron.,* vol. 6, pp. 338–345, July 1991.
[10] R. Oruganti, J. J. Yang, and F. C. Lee, "Implementation of optimal trajectory control of series resonant converters," *IEEE Trans. Power Electron.,* vol. 3, pp. 318–327, July 1988.
[11] J. M. Carrasco, F. Gordillo, L. G. Franquelo, and F. R. Rubio, "Control of resonant converters using the LQG/LTR method," in *Proc. IEEE PESC,* 1992, pp. 814–821.
[12] P. P. Bonissone, V. Badami, K. H. Chiang, P. S. Khedkar, K. W. Marcelle, and M. J. Schutten, "Industrial applications of fuzzy logic at general electric," *Proc. IEEE,* vol. 83, pp. 450–465, Mar. 1995.
[13] S. R. Sanders, G. C. Verghese, and D. E. Cameron, "Nonlinear control of switching power converters," *Control—Theory and Advanced Technology,* vol. 5, no. 4, pp. 601–617, 1989.
[14] S. R. Sanders and G. C. Verghese, "Lyapunov-based control for switching power converters," in *Proc. IEEE PESC,* 1990, pp. 51–58.
[15] L. A. Kamas and S. R. Sanders, "Parameter and state estimation in power electronic circuits," *IEEE Trans. Circuits Syst. I,* vol. 40, no. 12, pp. 920–928.
[16] A. M. Stankovic, "A dissipativity-based controller for series resonant dc/dc converters," in *Proc. IEEE PESC,* 1996, pp. 1844–1849.
[17] A. M. Stankovic, D. J. Perreault, and K. Sato, "Analysis and experimentation with dissipative nonlinear controllers for series resonant dc/dc converters," in *Proc. IEEE PESC,* 1997, pp. 679–685.
[18] C. A. Jacobson, A. M. Stankovic, and G. Tadmor, "Design of robust controllers for resonant dc/dc converters," in *Proc. IEEE Conf. Control Applications,* Albany, NY, 1995, pp. 360–365.
[19] R. Ortega and G. Espinosa, "Torque regulation in induction motors," *Automatica,* vol. 29, no. 3, pp. 621–633, 1993.

[20] H. Nijmeijer and A. J. van der Schaft, *Nonlinear Dynamical Control Systems.* New York: Springer-Verlag, 1990.
[21] V. Vorperian and S. Cuk, "A complete dc analysis of the series resonant converter," in *Proc. IEEE PESC,* 1982, pp. 85–100.
[22] I. J. Perez-Arriaga, G. C. Verghese, and F. C. Schweppe, "Selective modal analysis I: Heuristic introduction," *IEEE Trans. Power Apparatus Syst.,* vol. 101, pp. 3117–3125, Sept. 1982.
[23] P. Kundur, *Power System Stability and Control.* New York: McGraw-Hill, 1994.
[24] H. K. Khalil, *Nonlinear Systems.* New York: Macmillan, 1992.
[25] P. V. Kokotovic, H. K. Khalil, and J. O'Reilly, *Singular Perturbation Methods in Control: Analysis and Design.* New York: Academic, 1986.
[26] R. M. Murray, M. Rathinam, and W. Sluis, "Differential flatness of mechanical control systems: A catalog of prototype systems" in *ASME Int. Mech. Engr. Congress,* Nov. 1995.
[27] H. Sira-Ramirez, R. Ortega, P. Martin, P. Rouchon, and R. Marquez, "Regulation of dc/dc power converters: A differential flatness approach," in *Proc. IFAC World Congress,* San Francisco, CA, July 1996, vol. 2b-17, pp. 43–48.

David J. Perreault (S'91–M'97) was born in North Providence, RI, on January 22, 1967. He received the B.S. degree from Boston University, Boston, MA, in 1989 and the S.M. and Ph.D. degrees from the Massachusetts Institute of Technology, Cambridge, in 1991 and 1997, all in electrical engineering.

He is currently a Post-Doctoral Researcher in the MIT Laboratory for Electromagnetic and Electronic Systems, where his work includes the investigation of new methods for the design and control of power electronic systems.

Dr. Perreault is a member of Tau Beta Pi, Sigma Xi, and the National Society of Professional Engineers.

Aleksandar M. Stanković (M'93) received the Dipl. Ing. and M.S. degrees from the University of Belgrade, Belgrade, Yugoslavia, in 1982 and 1986, respectively, and the Ph.D. degree from the Massachusetts Institute of Technology, Cambridge, in 1993, all in electrical engineering.

Since 1993, he has been with the Department of Electrical and Computer Engineering, Northeastern University, Boston, MA, and is presently an Associate Professor. His research interests are in modeling, estimation, and control problems in power electronics, electric drives, and power systems.

Dr. Stanković is a member of the IEEE Power Electronics, Control Systems, Industry Applications, Industrial Electronics, and Power Engineering Societies. He currently serves as an Associate Editor for the IEEE TRANSACTIONS ON CONTROL SYSTEMS TECHNOLOGY.

Kenji Sato (S'97–M'98) was born in Toko, Japan, on May 8, 1966. He received the B.S. and M.E. degrees in electrical engineering from Waseda University, Tokyo, Japan, in 1989 and 1991, respectively, and the S.M. degree in electrical engineering from the Massachusetts Institute of Technology (MIT), Cambridge, in 1997.

He joined the Central Japan Railway Company (JR Central), Tokyo, where he has been engaged in the development and design of the power conversion systems of the Shinkansen Train (a bullet train). From 1995 to 1997, he was involved in research on paralleled power converters at MIT. He is currently working on a next-generation high-speed train project at JR Central.

Mr. Sato is a member of the Institute of Electrical Engineers of Japan.